A comparative analysis of in-medium spectral functions for $N(940)$ and $N^*(1535)$ in real-time thermal field theory

Sabyasachi Ghosh[*]

[*]Instituto de Fisica Teorica, Universidade Estadual Paulista, Rua Dr. Bento Teobaldo Ferraz, 271, 01140-070 Sao Paulo, SP, Brazil

Abstract

In the real-time thermal field theory, the nucleon self-energy at finite temperature and density is evaluated where an extensive set of pion-baryon (πB) loops are considered. On the other side the in-medium self-energy of $N^*(1535)$ for πN and ηN loops is also determined in the same framework. The detail branch cut structures for these different πB loops for nucleon $N(940)$ and πN, ηN loops for $N^*(1535)$ are addressed. Using the total self-energy of $N(940)$ and $N^*(1535)$, which contain the contributions of their corresponding loop diagrams, the complete structures of their in-medium spectral functions have been obtained. The Landau and unitary cut contributions provide two separate peak structures in the nucleon spectral function while $N^*(1535)$ has single peak structure in its unitary cuts. At high temperature, the peak structures of both at their individual poles are attenuated while at high density Landau peak structure of nucleon is completely suppressed and its unitary peak structure is tending to be shifted towards the melted peak of $N^*(1535)$. The nontrivial modifications of these chiral partners may indicate some association of chiral symmetry restoration.

1 Introduction

In the limit of massless quarks (u, d), QCD Lagrangian density for quark field ψ_f can be expressed in terms of its left and right handed components $\psi_f^{L,R} = \frac{1}{2}(1 \mp \gamma_5)\psi_f$ as

$$
\begin{aligned}
\mathcal{L}_{\text{QCD}} &= i \sum_{f=u,d} \overline{\psi}_f \gamma^\mu \partial_\mu \psi_f + .. \\
&= i \sum_{f=u,d} \overline{\psi}_f^R \gamma^\mu \partial_\mu \psi_f^R + i \sum_f \overline{\psi}_f^L \gamma^\mu \partial_\mu \psi_f^L + ..,
\end{aligned} \tag{1}
$$

which remains invariant under global $\text{SU}(2)_L \times \text{SU}(2)_R$ symmetry and leads to the conserved Noether currents $J_{L,R}^{\mu a} = \overline{\psi}_f^{L,R} \gamma^\mu \frac{\tau^a}{2} \psi_f^{L,R}$. This implies that chirality or handedness is preserved and the associated symmetry of the strong interaction in this limit is known as chiral symmetry.

The observable particles i.e. hadrons are eigenstates of parity and so it is useful to work with the vector and axial-vector Noether currents

$$
\begin{aligned}
J_{V,A}^{\mu a} &= J_R^{\mu a} \pm J_L^{\mu a} \\
&= \overline{\psi}_f \gamma^\mu \left\{ \begin{array}{c} \mathbf{1} \\ \gamma^5 \end{array} \right\} \frac{\tau^a}{2} \psi_f .
\end{aligned}
\tag{2}
$$

The triplet of charges $Q_{V,A}^a = \int d^3x J_{V,A}^{0a}(x)$ are the corresponding (quantum) generators of $\mathrm{SU}(2)_R \times \mathrm{SU}(2)_L$ which commute with the Hamiltonian of QCD

$$
[Q_{V,A}^a, H] = 0.
\tag{3}
$$

The states that from irreducible representation (basis) of the $\mathrm{SU}(2)_V$ group can be connected by

$$
Q_V |V_1\rangle = |V_2\rangle .
\tag{4}
$$

From Eq. (4) and (3) it follows immediately that

$$
\begin{aligned}
E_{V_1} &= \langle V_1 | H | V_1 \rangle \\
&= \langle V_1 | Q_V^\dagger H Q_V | V_1 \rangle \\
&= \langle V_2 | H | V_2 \rangle = E_{V_2} .
\end{aligned}
\tag{5}
$$

Thus the symmetry of Hamiltonian H is manifest in the degeneracies of the energy eigenstates corresponding to the irreducible representations of the symmetry group. Since $|V_1\rangle$ and $|V_2\rangle$ must be related to the ground state $|0\rangle$ through some appropriate creation operators ϕ_{V_1} and ϕ_{V_2} by the relations: $|V_1\rangle = \phi_{V_1}|0\rangle$, $|V_2\rangle = \phi_{V_2}|0\rangle$ and $Q_V \phi_{V_1} Q_V^\dagger = \phi_{V_2}$. On the basis of these relations, the Eq. (4) as well as Eq. (5) are satisfied only when [1] $Q_V|0\rangle = 0$, which was shown by Vafa and Witten [2]. Isospin symmetry i.e. $\mathrm{SU}(2)_V$ is consequently realized in the usual Wigner-Weyl mode which is reflected in the spectrum through the almost degenerate doublet of the proton and neutron, the triplet of the ρ^+, ρ^0, ρ^- etc. In addition to the vector charges, if the axial charges also annihilate the vacuum i.e. $Q_A^a|0\rangle = 0$, parity doublets like scalar and pseudo scalar mesons (σ, π) or vector and axial vector mesons (ρ, a_1) should exist in the spectrum. Although the vacuum hadronic spectra exhibit the absence of such kind of the doublets, which indicates $Q_A^a|0\rangle \neq 0$ by associating with the non-zero QCD vacuum, $\langle 0|\overline{\psi}_f \psi_f|0\rangle \neq 0$. These non-zero relations lead to *spontaneous* or *Dynamical* breaking of chiral symmetry (SBCS or DBCS) [3, 4, 5] even in the zero quark mass limit, which prevent to break chiral symmetry *explicitly*. Now under the extreme scenario of QCD matter produced in heavy ion experiments at very high energy, this broken symmetry may be restored by melting down the quark condensate. Being associated with this chiral symmetry restoration (CSR), the non-degenerate spectra of chiral partners (σ, π), (ρ, a_1) etc. may approach towards the degenerate states under such an extreme state of QCD matter.

In the baryon sector, an equivalent scenario is expected for nucleon and its (lowest possible) chiral partner $N^*(1535)$. In this context, a comparative investigation of in-medium spectral function for $N(940)$ and $N^*(1535)$ may be very relevant and interesting. This phenomenology of the baryons are analyzed by various groups [6, 7, 8, 9, 10, 11, 12, 14] in different theoretical ways such

as linear sigma model [7], lattice QCD calculations [8, 9], QCD sum-rule approach [10, 11], instanton liquid model [12] etc. Here this article is intended to investigate this phenomenology via effective hadronic model, where the thermodynamical parts are governed by the real-time formalism of thermal field theory. According to the Refs. [5, 13], the CSR mechanism may be linked with the different possible spectral modifications of the chiral partners. Our aim is to search which one is preferred or indicated (may be partially) by our hadronic model calculation at finite temperature?

Next in the formalism part, the expression of thermal propagators as well as self-energies for $N(940)$ and $N^*(1535)$ are explicitly derived. In Sec. (3), the detailed numerical results are discussed and at last section the intention of the article is summarized.

2 Formalism

2.1 Propagators of $N(940)$ and $N^*(1535)$ in the medium

We begin with the 11 component of the nucleon propagator in real-time thermal field theory (RTF),

$$S_{11}^{(0)}(k) = (\not{k} + m_N)D_{11}^{(0)}(k) \; , \tag{6}$$

where

$$
\begin{aligned}
D_{11}^{(0)}(k) &= \frac{-1}{k^2 - m_N^2 + i\eta} - 2\pi i F_k(k_0)\delta(k^2 - m_N^2) \; , \\
&\qquad \text{with} \;\; F_k(k_0) = n_k^+ \theta(k_0) + n_k^- \theta(-k_0) \\
&= -\frac{1}{2\omega_k}\left(\frac{1 - n_k^+}{k_0 - \omega_k + i\eta} + \frac{n_k^+}{k_0 - \omega_k - i\eta} \right. \\
&\qquad\qquad \left. - \frac{1 - n_k^-}{k_0 + \omega_k - i\eta} - \frac{n_k^-}{k_0 + \omega_k + i\eta} \right) \; .
\end{aligned} \tag{7}
$$

Here $n_k^\pm(\omega_k) = 1/\{e^{\beta(\omega_k \mp \mu_N)} + 1\}$ denote Fermi-Dirac distribution functions of nucleon anti-nucleon respectively with energy $\omega_k = \sqrt{\vec{k}^2 + m_N^2}$.

With the help of the diagonalization technique this 11 component of thermal propagator can be transformed to the diagonal element [15, 16],

$$\overline{S}^{(0)}(k) = (\not{k} + m_N)\frac{-1}{k^2 - m_N^2 + i\eta} \; , \tag{8}$$

which is exactly same with free vacuum propagator. The Dyson equation in terms of the diagonal elements can be represented as [15, 16]

$$\overline{S} = \overline{S}^{(0)} - \overline{S}^{(0)}\overline{\Sigma}_N \; \overline{S} \; , \tag{9}$$

where $\overline{S}(k)$ and $\overline{\Sigma}(k)$ are the diagonal element of complete propagator and self-energy of nucleon respectively. Taking scalar part of particle propagation only, we get the simplified form of nucleon spectral function,

$$
\begin{aligned}
A_N(k, T, \mu_N) &= \mathrm{Im}\overline{S}(k, T, \mu_N) \\
&= \frac{-\mathrm{Im}\overline{\Sigma}_N(k, T, \mu_N)}{(k_0 - \omega_k - \mathrm{Re}\overline{\Sigma}_N(k, T, \mu_N))^2 + (\mathrm{Im}\overline{\Sigma}_N(k, T, \mu_N))^2} \; ,
\end{aligned} \tag{10}
$$

3
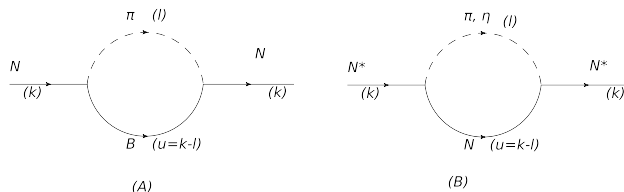
Figure 1: Self-energy diagrams of $N(940)$ (A) and $N^*(1535)$ (B) for respectively πB and πN (or ηN) loops.

where $\overline{\Sigma}_N = \text{Re}\overline{\Sigma}_N + i\text{Im}\overline{\Sigma}_N$. The $N^*(1535)$ will also have a similar form of spectral function where the nucleon self-energy $\overline{\Sigma}_N$ will be replaced by it's own self-energy, $\overline{\Sigma}_{N^*}$.

2.2 self-energies of $N(940)$ and $N^*(1535)$ in the medium

Next our aim is to calculate the thermal self-energy of $N(940)$ and $N^*(1535)$ in RTF. Inside a hot and dense nuclear matter, the nucleon may be propagated via different intermediate πB loops, where B stand for different higher mass baryons including nucleon itself. An extensive set of 4-star baryon resonances with spin one-half and three-half are taken in this work. They are $N(980)$, $\Delta(1232)$, $N^*(1440)$, $N^*(1520)$, $N^*(1535)$, $\Delta^*(1600)$, $\Delta^*(1620)$, $N^*(1650)$, $\Delta^*(1700)$, $N^*(1700)$, $N^*(1710)$, $N^*(1720)$; where their masses (in MeV) are displayed inside the brackets. The diagram 1(A) has shown the nucleon self-energy for πB loop. The 11 component of self-energy can be represented as

$$\Sigma_N^{11}(k, T, \mu_N) = -i \int \frac{d^4l}{(2\pi)^4} L(k,l) D_{11}(l, m_\pi, T)$$
$$D_{11}(u = k - l, m_B, T, \mu_N) , \qquad (11)$$

where $D_{11}(l, m_\pi, T)$, $D_{11}(u = k - l, m_B, T, \mu_N)$ are scalar part of the thermal propagators for pion and baryon respectively. The two vertices and the numerator parts of the propagators are contained in the factor $L(k,l)$. All the baryon chemical potentials are supposed to be same with nucleon chemical potential μ_N. Similar to the propagator matrix, the self-energy matrix can also be diagonalized into a single component. The diagonal element and 11 component are related as [15, 16]

$$\text{Im}\overline{\Sigma}_N(k) = \coth\left\{\frac{\beta(k_0 - \mu_N)}{2}\right\} \text{Im}\Sigma_N^{11}(k)$$
$$\text{Re}\overline{\Sigma}_N(k) = \text{Re}\Sigma_N^{11}(k) \qquad (12)$$

Taking the l_0 integration in (11) and then using the relation (12), the imaginary and real part of the diagonal element can be obtained as

$$\text{Im}\overline{\Sigma}_N(k) = \pi \int \frac{d^3l}{(2\pi)^3} \frac{1}{4\omega_l \omega_u}$$
$$[L_1\{(1 + n_l - n_u^+)\delta(k_0 - \omega_l - \omega_u)$$
$$+(-n_l - n_u^-)\delta(k_0 - \omega_l + \omega_u)\}$$

4

$$+L_2\{(n_l + n_u^+)\delta(k_0 + \omega_l - \omega_u)$$
$$+(-1 - n_l + n_u^-)\delta(k_0 + \omega_l + \omega_u)\}] \tag{13}$$

and

$$\mathrm{Re}\overline{\Sigma}_N(k) = \mathcal{P}\left[\int \frac{d^3l}{(2\pi)^3}\frac{1}{4\omega_l\omega_u}\left\{\frac{L_1(1 + n_l) - L_3 n_u^+}{k_0 - \omega_l - \omega_u}\right.\right.$$
$$+\frac{-n_l L_1 - n_u^- L_4}{k_0 - \omega_l + \omega_u)} + \frac{L_2 n_l + L_3 n_u^+}{k_0 + \omega_l - \omega_u}$$
$$\left.\left.+\frac{-n_l L_2 + (-1 + n_u^-)L_4}{k_0 + \omega_l + \omega_u}\right\}\right] \tag{14}$$

where $\omega_l = \sqrt{\vec{l}^2 + m_\pi^2}$, $\omega_u = \sqrt{(\vec{k} - \vec{l})^2 + m_B^2}$ and L_i , $i = 1,...4$ denote the values of $L(l_0)$ for $l_0 = \omega_l,\ -\omega_l,\ q_0 - \omega_l,\ q_0 + \omega_l$ respectively. The $\mathcal{P}$ indicates the principal value of the integrals. Here $n_u^\pm$ stand for Fermi-Dirac distribution functions of the baryons and anti-baryons while n_l denotes the Bose-Einstein distribution functions of the pion in the medium. The range of the different branch cuts in k_0-axis are ($-\infty$ to $-\{\vec{k}^2 + (m_\pi + m_B)^2\}^{1/2}$) for unitary cut in negative k_0-axis, ($-\{\vec{k}^2 + (m_B - m_\pi)^2\}^{1/2}$ to $\{\vec{k}^2 + (m_B - m_\pi)^2\}^{1/2}$) for Landau cut and ($\{\vec{k}^2 + (m_\pi + m_B)^2\}^{1/2}$ to ∞) for unitary cut in positive k_0-axis. Owing to the different δ functions in Eq. (13), the imaginary part of the nucleon self-energy become non-zero in the above regions. We will mainly focus on the unitary and Landau cut contributions of $\mathrm{Im}\overline{\Sigma}$ in positive k_0-axis, which are originated from the first and third term of Eq. (13) respectively. They can be simplified as

$$\mathrm{Im}\overline{\Sigma}_N(k) = \frac{1}{16\pi\vec{k}}[\int_{\omega_l^-}^{\omega_l^+} d\omega_l L_1\{1 + n_l(\omega_l) - n_u^+(k_0 - \omega_l)\}$$
$$+\int_{\widetilde{\omega}_l^+}^{\widetilde{\omega}_l^-} d\widetilde{\omega}_l L_2\{n_l(\widetilde{\omega}_l) + n_u^+(k_0 + \widetilde{\omega}_l)\}] \tag{15}$$

where $\omega_l^\pm = \frac{R^2}{2k^2}(k_0 \pm \vec{k}W)$, $\widetilde{\omega}_l^\pm = \frac{R^2}{2k^2}(-k_0 \pm \vec{k}W)$ with $W = \sqrt{1 - \frac{4m_\pi^2 k^2}{R^4}}$ and $R^2 = k^2 + m_\pi^2 - m_B^2$.

The vacuum part of $\mathrm{Re}\overline{\Sigma}_N$ is not written in the Eq.(14) as we are only interested in the medium part. That divergent quantity is traditionally assumed to take part for generating physical mass of nucleon.

The typical form of the $BN\pi$ interaction (effective) Lagrangian densities are as follows [17]

$$\mathcal{L} = \frac{f}{m_\pi}\overline{\psi}_B\gamma^\mu\left\{\begin{array}{c} i\gamma^5 \\ 1 \end{array}\right\}\psi_N\partial_\mu\pi + \text{h.c. for } J_B^P = \frac{1}{2}^\pm\ ,$$
$$= \frac{f}{m_\pi}\overline{\psi}_B^\mu\left\{\begin{array}{c} 1 \\ i\gamma^5 \end{array}\right\}\psi_N\partial_\mu\pi + \text{h.c. for } J_B^P = \frac{3}{2}^\pm\ . \tag{16}$$

The coupling constants f/m_π for different $BN\pi$ interactions have been fixed from the experimental vacuum widths of corresponding $B \to N\pi$ decays. The free parameter of the Rarita-Schwinger field (ψ_B^μ) is chosen as -1 [18]. Using

5

Table 1: From the left to right columns, the table contain the baryons, their spin-parity quantum numbers J_B^P, isospin I_B, total decay width Γ_{tot}, decay width in $N\pi$ channels $\Gamma_{B\to N\pi}$ or $\Gamma_B(m_B)$ in Eq. (19) (brackets displaying its Branching Ratio) and at the last coupling constants f/m_π.

Baryons	J_B^P	I_B	Γ_{tot}	$\Gamma_{B\to N\pi}$ (B.R.)	f/m_π
$\Delta(1232)$	$\frac{3}{2}^+$	$3/2$	0.117	0.117 (100%)	15.7
$N^*(1440)$	$\frac{1}{2}^+$	$1/2$	0.300	0.195 (65%)	2.5
$N^*(1520)$	$\frac{3}{2}^-$	$1/2$	0.115	0.069 (60%)	11.6
$N^*(1535)$	$\frac{1}{2}^-$	$1/2$	0.150	0.068 (45%)	1.14
$\Delta^*(1600)$	$\frac{3}{2}^+$	$3/2$	0.320	0.054 (17%)	3.4
$\Delta^*(1620)$	$\frac{1}{2}^-$	$3/2$	0.140	0.035 (25%)	1.22
$N^*(1650)$	$\frac{1}{2}^-$	$1/2$	0.150	0.105 (70%)	1.14
$\Delta^*(1700)$	$\frac{3}{2}^-$	$3/2$	0.300	0.045 (15%)	9.5
$N^*(1700)$	$\frac{3}{2}^-$	$1/2$	0.100	0.012 (12%)	2.8
$N^*(1710)$	$\frac{1}{2}^+$	$1/2$	0.100	0.012 (12%)	0.35
$N^*(1720)$	$\frac{3}{2}^+$	$1/2$	0.250	0.028 (11%)	1.18

the Lagrangian densities from Eq. (16), one can easily derive

$$
\begin{aligned}
L(k,l) & = -\left(\frac{f}{m_\pi}\right)^2 \slashed{l}(\slashed{k}-\slashed{l}-Pm_B)\slashed{l} \qquad \text{for } J_B^P = \frac{1}{2}^\pm , \\
& = -\left(\frac{f}{m_\pi}\right)^2 (\slashed{k}-\slashed{l}+Pm_B)l_\mu l_\nu \left\{-g^{\mu\nu}\right. \\
& \quad +\frac{1}{3}\gamma^\mu\gamma^\nu + \frac{2}{3m_B^2}(k-l)^\mu(k-l)^\nu \\
& \quad \left. +\frac{1}{3m_B}(\gamma^\mu(k-l)^\nu - (k-l)^\mu\gamma^\nu)\right\} \\
& \qquad\qquad\qquad\qquad \text{for } J_B^P = \frac{3}{2}^\pm .
\end{aligned}
\tag{17}
$$

To avoid the complexity of dealing with Dirac structure of self-energy as well as propagator, we have followed the simplified technique of Ref. [19], where total self-energy has been identified as summation of the coefficients of γ^0 and unit matrix. Therefore, ignoring the coefficients of γ^i for simplification and adding the coefficients of γ^0 and unit matrix [19], we have

$$
\begin{aligned}
L(k,l) & = -\left(\frac{f}{m_\pi}\right)^2 \left\{\left(k\cdot l - l^2\right)l_0 - Pl^2 m_B\right\} \\
& \qquad\qquad \text{for } J_B^P = \frac{1}{2}^\pm , \\
& = -\left(\frac{f}{m_\pi}\right)^2 \frac{2}{3m_B^2}\left\{\left(k\cdot l - l^2\right)^2 - l^2 m_B^2\right\}(k_0 \\
& \quad - l_0 + Pm_B) \quad \text{for } J_B^P = \frac{3}{2}^\pm .
\end{aligned}
\tag{18}
$$

These vertex factors $L(k,l)$ have to be put in Eq. (11) to obtain numerical values of nucleon self-energy.

The Lagrangian densities in (16) are not displaying its isospin structures. For $J_B^P = \frac{1}{2}^\pm$ and $J_B^P = \frac{3}{2}^\pm$ these isospin structures should be $\overline{\psi}\vec{\tau}\cdot\vec{\pi}\psi$ and $\overline{\psi}\vec{T}\cdot\vec{\pi}\psi$ respectively, where $\vec{T}$ and $\vec{\tau}$ stand for the usual spin 3/2 transition and Pauli operator. These isospin structures provide appropriate isospin factors, which have to be multiplied with the expressions of corresponding πB loop diagrams. The isospin factor for πN or πN^* loops is $I_{N\to\pi N, N^*} = 3$ and for the $\pi\Delta$ or $\pi\Delta^*$, it is $I_{N\to\pi\Delta,\Delta^*} = 2$.

Next we calculate vacuum width of different baryons in the $N\pi$ decay channel to fix their corresponding coupling constants f/m_π. With the help of the Lagrangian densities, vacuum decay width of baryons B for $N\pi$ channel can be obtained as

$$
\begin{aligned}
\Gamma_B(m_B) & = \frac{I_{N^*\to\pi N}}{2J_B+1}\left(\frac{f}{m_\pi}\right)^2 \frac{|\vec{p}_{cm}|}{2\pi m_B}[2m_B|\vec{p}_{cm}|^2 \\
& \quad + m_\pi^2(\omega_N - Pm_N)] \quad \text{for } J_B^P = \frac{1}{2}^\pm , \\
& = \frac{I_{\Delta,\Delta^*\to\pi N}}{2J_B+1}\left(\frac{f}{m_\pi}\right)^2 \frac{|\vec{p}_{cm}|^3}{3\pi m_B}[\omega_N
\end{aligned}
$$

$$+ Pm_N] \quad \text{for} \quad J_B^P = \frac{3^\pm}{2} \tag{19}$$

where $|\vec{p}_{cm}| = \frac{\sqrt{\{m_B^2-(m_N+m_\pi)^2\}\{m_B^2-(m_N-m_\pi)^2\}}}{2m_B}$ and $\omega_N = \sqrt{|\vec{p}_{cm}|^2 + m_N^2}$. The isospin factors are $I_{N^*\to\pi N} = 3$ and $I_{\Delta,\Delta^*\to\pi N} = 1$ for the $N\pi$ decay channels of N^* and Δ^* (or Δ) respectively. Putting the experimental values [20] of $\Gamma_B(m_B)$ in Eq. (19), the values of coupling constants f/m_π have been fixed, which are shown in Table (1).

For the self-energy calculation of $N^*(1535)$, the πN and ηN loops are mainly considered because approximately 45% and 40% [20] of its vacuum width ($\Gamma_{N^*} = 0.150$ GeV) are coming from these two decay channels (πN and ηN). Hence the total self-energy of $N^*(1535)$ is defined as

$$\overline{\Sigma}_{N^*} = \overline{\Sigma}_{N^*}^{\pi N} + \overline{\Sigma}_{N^*}^{\eta N} , \tag{20}$$

where $\overline{\Sigma}_{N^*}^{\pi N}$ and $\overline{\Sigma}_{N^*}^{\eta N}$ are the individual contributions for πN and ηN loops. They are diagrammatically shown in Fig. 1(B). In the imaginary part of self-energy for $T = 0$, the remaining part of vacuum width 0.022 GeV (15% branching ratio) are added with the numerical contributions of πN and ηN loops. The expressions of imaginary and real part of $\overline{\Sigma}_{N^*}^{\pi N}$ or $\overline{\Sigma}_{N^*}^{\eta N}$ will be similar with Eq. (13) and (14) respectively, where $\omega_l = \{\vec{l}^2 + m_{\pi,\eta}^2\}^{1/2}$ (for π and η respectively)and $\omega_u = \{(\vec{k}-\vec{l})^2 + m_N^2\}^{1/2}$ will be replaced only. Using Lagrangian density from (16) for $J_B^P = \frac{1}{2}^-$, one can find the factor $L(k,l)$ for πN loop as

$$L(k,l) = -I_{N^*\to\pi N} \left(\frac{f}{m_\pi}\right)^2 \left\{ \left(k\cdot l - l^2\right) l_0 + l^2 m_N \right\} . \tag{21}$$

Again using the same Lagrangian density, where π field only be replaced by η field, we can exactly receive same expression of $L(k,l)$ excluding the isospin factor ($I_{N^*\to\pi N} = 3$). The corresponding coupling constant has also be replaced as it has been fixed from the experimental decay width of $N^*(1535)$ in its $N\eta$ channel.

To include the in-medium effect of N in the πN or ηN loop, the modified $N^*(1535)$ self-energy can be defined as (similar technique is used for J/ψ in Ref. [21])

$$\overline{\Sigma}_{N^*}^{\pi,\eta N}(k, m_N, T, \mu_N) = \int_0^\infty dM^2 \overline{\Sigma}_{N^*}^{\pi,\eta N}(k, M, T, \mu_N)$$
$$\left\{ \frac{A_N(u_0, \vec{u}, T, \mu_N)}{\int_0^\infty dM^2 A_N(u_0, \vec{u}, T, \mu_N)} \right\} , \tag{22}$$

where $M^2 = u_0^2 - \vec{u}^2$. This modified expression after folding by nucleon spectral function at finite T and μ_N can be restored to its previous form (i.e. the form without folding) if the quantity inside $\{..\}$ of Eq. (22) is replaced by $\delta(M^2 - m_N^2)$.

3   Results and discussion

Let us start with the results of different invariant mass distribution of imaginary part of nucleon self-energy for different πB loops. In the Fig. (2) the
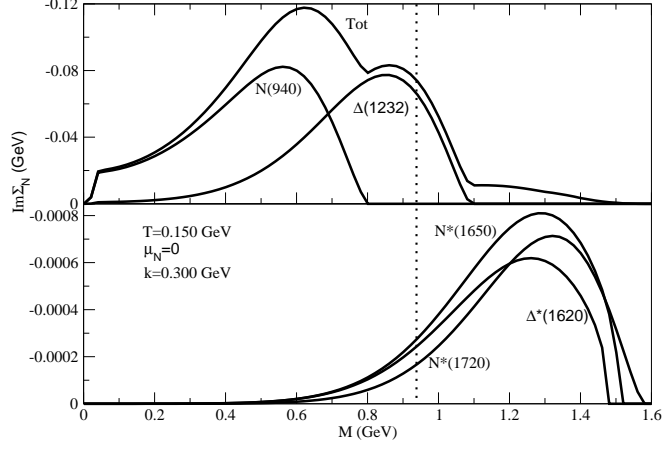
Figure 2: Imaginary part of nucleon self-energy for different πB loops. $B = \Delta^*(1620)$, $N^*(1650)$, $N^*(1720)$ are shown in lower panel while $B = N(940)$, $\Delta(1232)$ and total of all loops are displayed in upper panel.
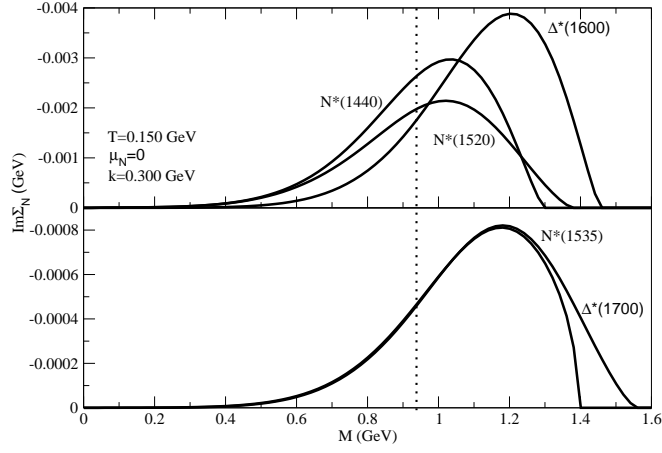

Figure 3: Same as Fig. (2) for rest of the baryons $B = N^*(1440)$, $N^*(1520)$, $\Delta^*(1600)$ (upper panel) and $B = N^*(1535)$, $\Delta^*(1700)$ (lower panel).
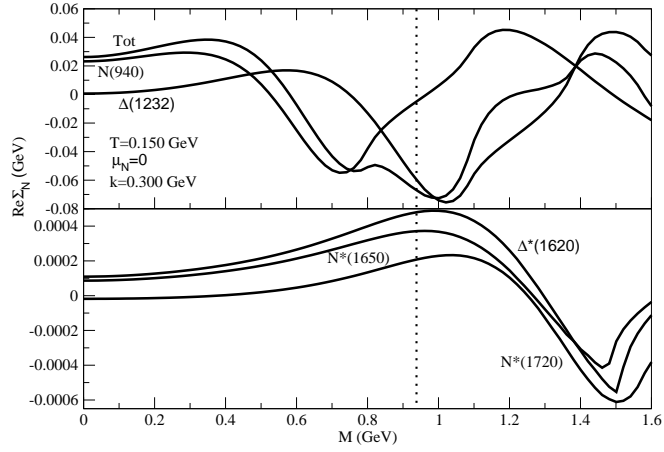
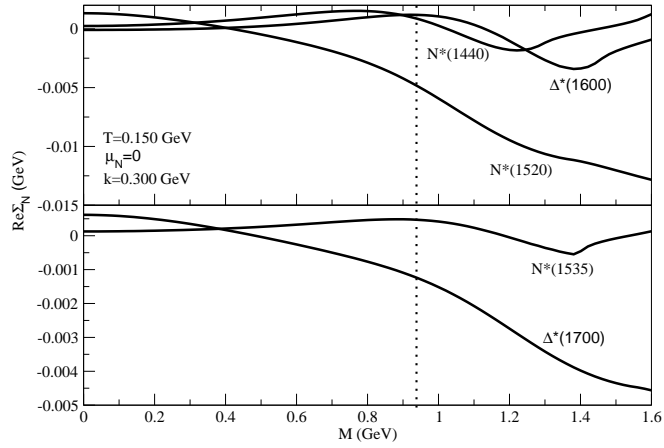Figure 4: The corresponding results of Fig. (2) for the real part of nucleon self-energy.

Figure 5: The corresponding results of Fig. (3) for the real part of nucleon self-energy.
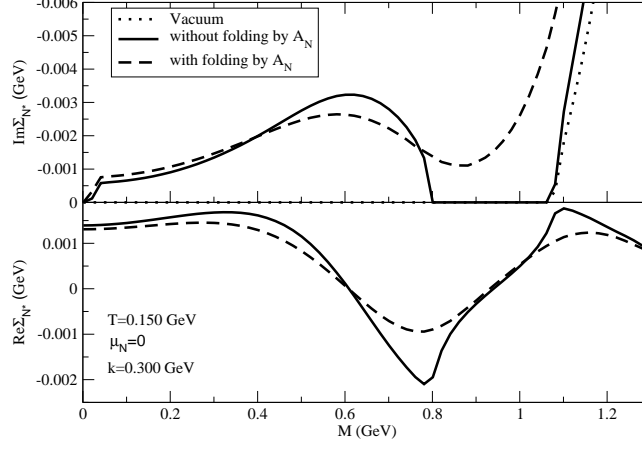
Figure 6: Imaginary (upper panel) and real (lower panel) part of $N^*(1535)$ self-energy for πN loop. Dotted line exhibits the vacuum strength of $\mathrm{Im}\Sigma_{N^*}$ coming from unitary cuts only. The solid line of $\mathrm{Im}\Sigma_{N^*}$ reveals two distinct regions of Landau and unitary cuts, which are overlapped after folding $\mathrm{Im}\Sigma_{N^*}$ by the in-medium nucleon spectral function, A_N. This is shown in dashed line.
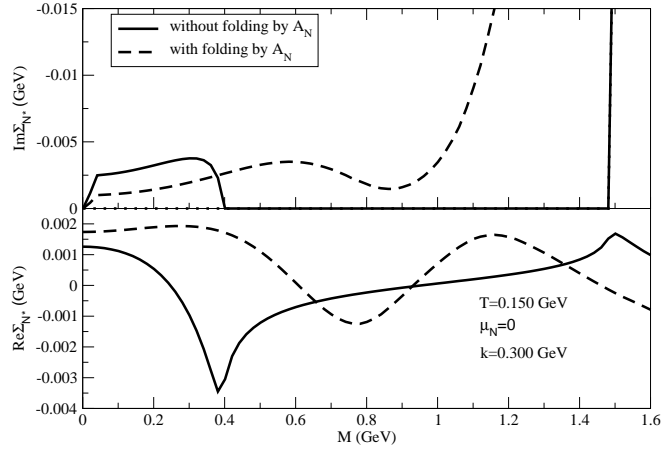
Figure 7: Imaginary (upper panel) and real (lower panel) part of $N^*(1535)$ self-energy for ηN loop. Same quantities of Fig. (6) are represented by solid and dashed lines for ηN loop.
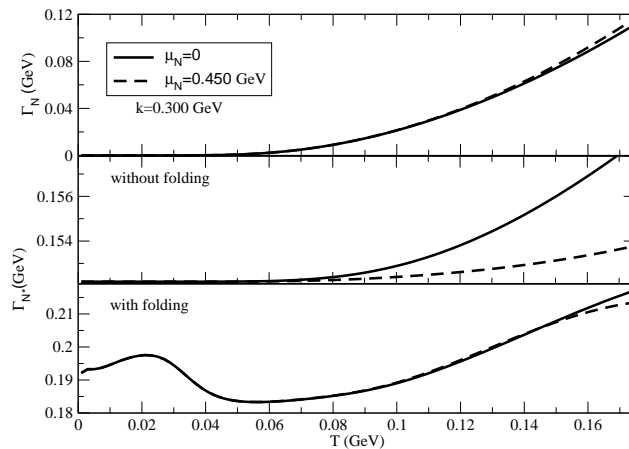
11

Figure 8: The temperature dependence of Γ_N (upper panel) and Γ_{N^*} without (middle panel) and with (lower panel) folding by the in-medium spectral function, A_N.

results for baryons $B = N(940)$, $\Delta(1232)$ (upper panel) and $B = \Delta^*(1620)$, $N^*(1650)$, $N^*(1720)$ (lower panel) are shown whereas the Fig. (3) demonstrates the results for baryons $B = N^*(1440)$, $N^*(1520)$, $\Delta^*(1600)$ (upper panel) and $B = N^*(1535)$, $\Delta^*(1700)$ (lower panel). All these results are generated for fixed value of temperature ($T = 0.150$ GeV), nucleon chemical potential ($\mu_N = 0$) and nucleon momentum ($\vec{k} = 0.300$ GeV). The numerical strength for the $B = N^*(1700)$ and $N^*(1710)$ are so low that they are not displayed with the other baryons. The total contribution coming from all the loops is displayed in the upper panel of Fig. (2). The Landau regions for different loops are clearly recognized from the sharp ending of solid lines for each loops. For example the Landau region of the πN loop is ($M = 0$ to $m_N - m_\pi$ i.e. 0 to 0.8 GeV). The corresponding results of real part for different baryons are shown in Fig. (4) and (5). The contributions imaginary or real part of nucleon self-energy at its pole have been marked by dotted line in all of the graphs.

Similarly the imaginary (upper panel) and real (lower panel) part of $N^*(1535)$ self-energy for πN and ηN loops are displayed in Figs. (6) and (7) respectively. From the solid line of the figures (in the upper panel), the Landau and unitary regions are distinctly observed. However, their thresholds have been overlapped with each other after the folding by the in-medium spectral function of nucleon, A_N. The Eq. (22) generates this with-folding results, which are shown in dashed line in Fig. (6) and (7). The thermal width Γ_N for $N(940)$ and Γ_{N^*} for $N^*(1535)$ are extracted from the pole contributions of their corresponding total imaginary part of self-energy. For two different values of μ_N, the T dependence of Γ_N (upper panel), Γ_{N^*} without (middle panel) and with (lower panel) folding are presented in Fig. (8). This non-zero $\Gamma_N(T, \mu_N = 0)$ may have very important role in different relevant quantities (e.g. in shear viscosity [22]), estimated even for the baryon free matter, produced at RHIC or LHC experiments.

The total $N(940)$ self-energy contain the contributions of all of the πB loops whereas the total $N^*(1535)$ self-energy is composed of πN and ηN loops. Using
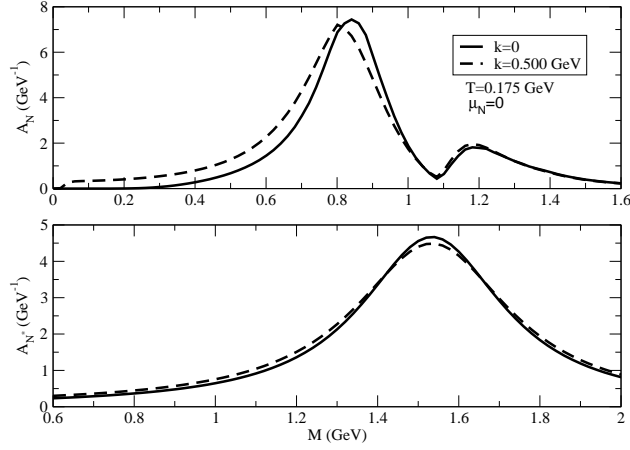
Figure 9: The spectral function of $N(940)$ (upper panel) and $N^*(1535)$ (lower panel) for two different values of $\vec{k}$.
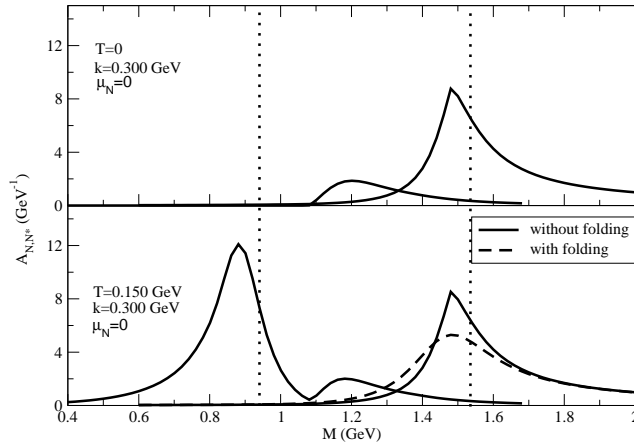

Figure 10: The spectral function of $N(940)$ and $N^*(1535)$ for $T = 0$ (upper panel) and $T = 0.150$ GeV (lower panel).
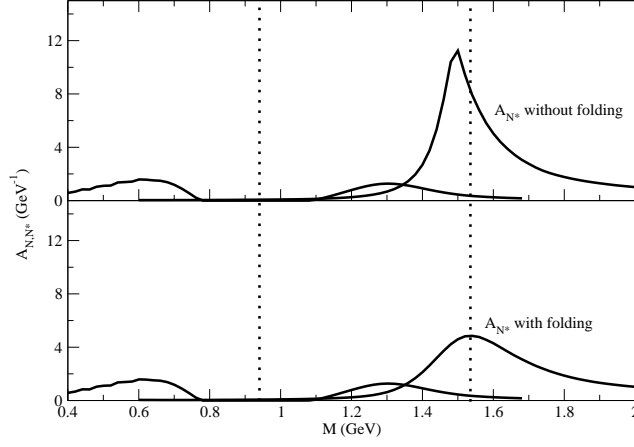
Figure 11: The spectral function of $N(940)$ and $N^*(1535)$ for $T = 0$, $\mu_N = 0.976$ GeV and $\rho = \rho_0$. In the upper and lower panel, the results of A_{N^*} without and with folding (by A_N) are shown.
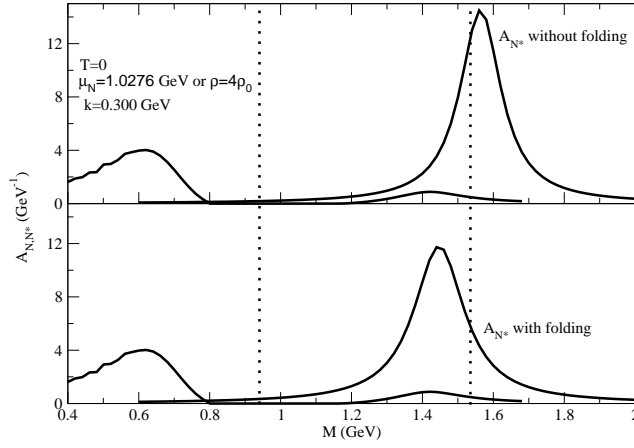

Figure 12: The spectral function of $N(940)$ and $N^*(1535)$ for $T = 0$, $\mu_N = 1.0276$ GeV and $\rho = 4\rho_0$.

14

their total self-energy in the corresponding expression of their spectral functions like Eq. (10), we will get the explicit in-medium structure of their spectral functions. The in-medium spectral functions of $N(940)$ (upper panel) and $N^*(1535)$ (lower panel) for two different values of three momentum $\vec{k}$ are shown in Fig. (9). Unlike to vacuum case, the spectral function at finite temperature become the function of k_0 and $\vec{k}$ independently which is numerically illustrated in Fig. (9). The effect of temperature on their spectral functions is presented in Fig. (10) by displaying the results for $T = 0$ (upper panel) and $T = 0.150$ GeV (lower panel). As the threshold $(m_\pi + m_B)$ of unitary cuts of the nucleon self-energy is far away from the nucleon pole, a small magnitude of vacuum spectral function is obtained in the upper panel of Fig. (10). Since the nucleon pole is situated within the region of Landau cuts, therefore at finite T, a good Breit-Wigner type structure is produced along with the small structures coming from the unitary cut contributions. This is displayed in lower panel of Fig. (10). Now for $N^*(1535)$ spectral function, the unitary cuts play a major role in vacuum as well as in medium as its pole is situated within the unitary cuts for πN and ηN loop diagrams. Due to folding by in-medium nucleon spectral function, the thermal width of $N^*(1535)$ increases noticeably which is already shown in the lower panel of Fig. (8). Hence the peak structure of $N^*(1535)$ spectral function melts down after this folding which is denoted by dash line in the lower panel of Fig. (10). The dotted lines are used to mark the bare pole positions of $N(940)$ and $N^*(1535)$. At $T = 0$ and $\mu_N = 0.976$ GeV or $\rho = \rho_0$ (where $\rho_0 = 0.16/\text{fm}^3$ is the nuclear matter saturation density), the modified spectral functions of $N(940)$ and $N^*(1535)$ are presented in Fig. (11) where the peak structure of nucleon spectral function is completely suppressed. The peak of $N^*(1535)$ spectral function is slightly enhanced from its vacuum spectral function because its thermal width will face the Pauli suppression dominantly at $T = 0$. Although this peak strength has been slightly diminished after the folding, which can be observed in the lower panel of Fig. (11). Again the peak of the small spectral strength for $N(940)$, which is coming from its unitary cut contributions, is shifted towards the peak of the $N^*(1535)$ spectral function. At very high density their peak positions may be coincided with each other. This is shown in the lower panel of Fig. (12).

Our first aim of this work is to investigate in-medium modifications of $N(940)$ and $N^*(1535)$ spectral functions, whose vacuum strengths are directly linked with the experimental inputs by fixing coupling constants of effective Lagrangian densities. Analyzing the detailed branch cuts of their self-energies in RTF, their in-medium spectral profiles are exhibiting some non-trivial modifications. Our next aim is to search any indication of CSR from their non-trivial modifications. We should keep in mind that in the effective hadronic model, the masses of chiral partners does not directly contain the information of temperature dependent quark condensate, which is nicely adopted in other chiral models like NJL, LSM etc. Hence, a transparent indication of parity doublet may not be found as demonstrated in the different chiral models. However, it is definitely an interesting to search it in effective hadronic model approach, whose richness is the fixing of interaction strengths via experimentally observed decay widths. During this searching of link between CSR and these non-trivial modifications of $N(940)$ and $N^*(1535)$ spectral functions, the conclusions of our hadronic model calculation in RTF are as follows. During increase of temperature, the Landau

peak strength of $N(940)$, which was completely absent in vacuum, may be approaching to be equal with the attenuated unitary peak strength of $N^*(1535)$. Whereas, during increase of density (at $T = 0$), the Landau peak of $N(940)$ is hardly suppressed and its unitary peak is shifted towards the unitary peak of $N^*(1535)$. Following the statements mentioned in Refs. [5, 13] regarding the possibilities spectral modifications of chiral partners to associate CSR, these approaching towards the equal peak strength (at high temperature) and positions (at high density) of these chiral partners may have some relation with CSR.

4 Summary and conclusion

To summarize, the in-medium self-energy of nucleon and it's chiral partner $N^*(1535)$ are evaluated in the RTF. An extensive set of pion-baryon loops are taken for the nucleon self-energy calculation. On the other hand πN and ηN loops are considered for the $N^*(1535)$. After summing all the respective loop contributions for $N(940)$ and $N^*(1535)$, their total self-energies have been determined which provide them the complete structures of in-medium spectral functions. Two distinct peak structure in the nucleon spectral function have been originated from it's Landau and unitary cut contributions whereas $N^*(1535)$ acquires a single peak structure from its unitary cuts. At high temperature, the spectral profile of both are broadened with their attenuated peak structures. At high density and $T = 0$, the peak structure of nucleon spectral function, coming from the Landau cuts, is completely suppressed from its pole position. Along with this suppression of the Landau peak, the unitary peak structure is tending to be shifted towards the attenuated peak of $N^*(1535)$. This comparative investigation of in-medium spectral functions for nucleon and its chiral partner $N^*(1535)$ exhibit a non-trivial modifications which may indicate some association of chiral symmetry restoration.

References

[1] Ta-Pei Cheng, Ling-Fong Li, *Gauge theory of elementary particle physics*, (New York : Oxford University Press, 1984).

[2] C. Vafa and E. Witten, Nucl. Phys. **B 234**, 173 (1984).

[3] R. S. Hayano and T. Hatsuda, Rev. Mod. Phys. **82** (2010) 2949.

[4] B. R. Holstein, Progress in Particle and Nuclear Physics 61 (2008) 3.

[5] V. Koch, Int. J. Mod. Phys. **E 6** (1997) 203, arXiv:nucl-th/9706075v2; arXiv:nucl-th/9512029.

[6] B.W. Lee, *Chiral Dynamics* (Gordon and Breach, New York, 1972).

[7] C. DeTar, T. Kunihiro, Phys. Rev. **D 2805** (1989) 39.

[8] C.E. DeTar, J.B. Kogut, Phys. Rev. Lett 339 (1987) 59; Phys. Rev. **D 2828** (1987) 36.

[9] S. Gottlieb, W. Liu, D. Toussaint, R.L. Renkin, R.L. Sugar, Phys. Rev. Lett. 1881 (1987) 59.

[10] D. Jido, N. Kodama, M. Oka, Phys. Rev. **D 4532** (1996) 54.

[11] D. Jido, M. Oka, A. Hosaka, Phys. Rev. Lett. 448 (1998) 80.

[12] T. Schafer, E.V. Shuryak, Phys. Lett. B 147 (1995) 356.

[13] J. I. Kapusta, E. V. Shuryak, Phys. Rev **D 49**, 9 (1994).

[14] S. Gallas, F. Giacosa and D. H. Rischke, Phys. Rev. **D 82** (2010) 014004; PoS CONFINEMENT 8 (2008) 089.

[15] R. L. Kobes and G. W. Semenoff, Nucl. Phys. 260, 714 (1985).

[16] S. Ghosh, *Probing spectral properties of hadrons in hot and dense hadronic matter* (Ph.D. Thesis) HBNI (India), 2012, http://www.hbni.ac.in/phdthesis/thesis_june2013 /PHYS04200704005_Sabyasachi_Ghosh.pdf

[17] M. Post, S. Leupold, U. Mosel, Nucl. Phys. **A 741**, 81 (2004).

[18] R.D. Peccei, Phys. Rev. 176 (1968) 1812.

[19] S. Ghosh, S. Sarkar, S. Mallik, Phys. Rev. **C 82** (2010) 045202.

[20] J. Beringer et al. (*Particle Data Group*) Phys. Rev. **D 86**, 010001 (2012).

[21] S. Ghosh, S. Mitra, S. Sarkar, Nucl. Phys. **A 917** (2013) 71.

[22] S. Ghosh, Phys. Rev. **C 89** (2014) 045201.